


**Insulator-to-metal transition in low-dimensional NbS<sub>3</sub> under pressure**Sergio Conejeros *Departamento de Química, Universidad Católica del Norte, Av. Angamos 0610, Antofagasta 1240000, Chile*Pere Alemany *Departament de Ciència de Materials i Química Física and Institut de Química Teòrica i Computacional (IQTCUB),  
Universitat de Barcelona, Martí i Franqués 1, 08028 Barcelona, Spain*Enric Canadell *Institut de Ciència de Materials de Barcelona (ICMAB-CSIC), Campus UAB, 08193 Bellaterra, Spain  
and Royal Academy of Sciences and Arts of Barcelona, Chemistry Section, La Rambla 115, 08002 Barcelona, Spain*

(Received 4 October 2023; revised 8 December 2023; accepted 11 December 2023; published 26 December 2023)

A first-principles study of the insulator-to-metal transition under pressure in NbS<sub>3</sub> is reported. In contrast with previous proposals, it is found that the transition is not due to a progressive closing of the initial band gap but to the inversion of the relative stability of two different polymorphs under pressure. The Fermi surface of the new metallic state under low pressure (polymorph V') is discussed, and the possible occurrence of as yet unknown incommensurate phases is suggested. The reason for the inversion of stability of the two polymorphs is discussed.

DOI: [10.1103/PhysRevB.108.214109](https://doi.org/10.1103/PhysRevB.108.214109)**I. INTRODUCTION**

Layered group IV and V transition-metal trichalcogenides (TMTCs) have been the object of continued attention because they exhibit challenging physical and chemical properties such as charge density waves (CDWs), superconductivity, easy chemical intercalation, etc. [1]. For instance, the CDW material NbSe<sub>3</sub> is one of the archetypal low-dimensional metals [2,3], and it was the first inorganic solid found to exhibit Fröhlich-type conductivity [4]. Whereas most of the group-IV MX<sub>3</sub> (*M* = Ti, Zr, Hf; *X* = S, Se, Te) layered systems are semiconducting [1,5], ZrTe<sub>3</sub> is metallic, exhibits a CDW at 63 K [6], and becomes superconducting under a moderate pressure of 5 GPa [7]. Interest in TMTCs has recently increased because of the possibility of preparing them as single-layer or few-layers-thick samples, and it has been shown that they may provide useful platforms for next-generation electronic and optoelectronic materials [5,8,9].

An appealing feature of some of these solids is their rich polymorphism [10]. For instance, NbS<sub>3</sub> has been shown to exist in many different polymorphs exhibiting substantially different physical behavior: semiconducting, metallic, CDWs, etc. For instance, the more usual polymorph, NbS<sub>3</sub>-I [11], exhibits TiS<sub>3</sub>-type structure [12] with a strong Nb-Nb dimerization and is a semiconductor with an ~1 eV band gap. However, another polymorph, NbS<sub>3</sub>-II, is a metal [13] with a layered structure [14] recalling that of NbSe<sub>3</sub> [15] and is one of the very few materials exhibiting three successive CDWs [16]. A recent theoretical study pointed out the possibility of topological effects in still another polymorph [10]. The structure and transport properties of NbS<sub>3</sub> are so subtly dependent on the synthetic procedure that it has been recently shown that

simply changing the nature of the transport agent in the chemical vapor transport process can lead to a different polymorph [17]. Under such conditions, pressure studies may be very useful. In fact, pressure can drive several transitions in the prototypical TiS<sub>3</sub> TMTC, which can evolve from insulating to superconducting [18,19]. An insulator to superconductor transition has been reported for HfS<sub>3</sub> at 17 GPa [20]. Pressure can also suppress the CDWs in NbSe<sub>3</sub> and stabilize a superconducting ground state [2].

Coming back to NbS<sub>3</sub>, it has been reported that a metallic state can be induced under pressure in the semiconducting NbS<sub>3</sub>-I phase [21,22]. The conductivity increases by five orders of magnitude for pressures around 5 GPa. In the most recent study, the pressure evolution of the Raman shifts as well as density functional theory calculations (DFT) were reported [21], and it was concluded that pressure progressively closes the initial gap to create partially filled bands and hence a metallic-type conductivity. However, we have reasonable concerns towards such a metallization mechanism. To begin with, 5 GPa seems to be a weak pressure to close an initial band gap of ~1 eV in a material with strong covalent bonds. For instance, closing a band gap of ~1 eV in the structurally related HfS<sub>3</sub> requires 17 GPa [20]. More importantly, since NbS<sub>3</sub> exhibits several different polymorphs, it seems more likely that a second polymorph, metallic and less stable than NbS<sub>3</sub>-I at ambient pressure, may be substantially stabilized by pressure and become the ground state of the system at around 4–6 GPa. In addition, the electronic structure of this experimentally observed moderate pressure metallic state has not yet been described in any detail.

In view of the unusual behavior of metallic TMTCs, we found it necessary to revisit the metallization mechanism

of NbS<sub>3</sub>-I under pressure and to characterize the electronic structure of this new metallic phase. In the present work, we report a detailed DFT study of the evolution of structurally strongly related NbS<sub>3</sub> polymorphs under pressure. We show that indeed a nondimerized and metallic NbS<sub>3</sub> polymorph becomes more stable than the initial semiconducting phase for pressures compatible with those of the experimental study, and we report a detailed study of the evolution of the Fermi surface of this metallic state under pressure.

## II. COMPUTATIONAL DETAILS

All calculations were carried out using first-principles density functional theory (DFT) [23,24]. The structural optimizations were carried out under hydrostatic pressures (0–15 GPa) using the *ab initio* CRYSTAL17 code [25–27]. Following previous work on NbS<sub>3</sub> polymorphs [10] where the performance of different functionals was tested, the hybrid functional HSE06 [28] was adopted. The all-electron atomic Gaussian basis sets used were 986-31-(631d)G [29] for Nb and pob-TZVP for S [30]. For the calculation of the Coulomb and exchange integrals, the tolerance factors of 7, 7, 7, 7, and 14 were used. The convergence criterion for the electronic energy was set at 10<sup>-7</sup> a.u. [31]. The reciprocal space integration used a mesh of (12 × 12 × 12) *k*-points in the irreducible Brillouin zone (BZ) chosen according to the Monkhorst-Pack scheme [32], and the convergence of the energy with the grid size was checked. In all geometry optimizations, the space group symmetry was kept fixed.

## III. TWO STRUCTURALLY RELATED POLYMORPHS

Shown in Fig. 1 are the calculated structures for two different polymorphs of NbS<sub>3</sub>—NbS<sub>3</sub>-I and NbS<sub>3</sub>-V—according to the labeling in Ref. [33], which mostly differ for the occurrence of dimerized and uniform Nb chains, respectively. NbS<sub>3</sub>-I is the usual semiconducting polymorph of NbS<sub>3</sub> [11,33]. The NbS<sub>3</sub>-V polymorph was experimentally reported more recently [33]. Both structures were found to be stable polymorphs according to DFT calculations [10]. These structures belong to the TiS<sub>3</sub> structure type [12]: they are built from NbS<sub>3</sub> chains of Nb atoms in a trigonal prismatic coordination such that the different trigonal prisms share the opposite triangular faces [see Fig. 1(d)]. It is important to notice that adjacent chains are shifted by  $b/2$ , where  $b$  is the repeat vector of the uniform chain, so that two additional interchain Nb-S bonds are created [see Fig. 1(c)] and, consequently, the Nb atoms are really found in a bicapped trigonal prismatic coordination. This leads to the formation of NbS<sub>3</sub> layers parallel to the (*ab*) plane of the crystal structure [Fig. 1(c)]. However, whereas the NbS<sub>3</sub> chains in polymorph V are uniform [i.e., there is only one Nb-Nb distance, Fig. 1(d)], those of polymorph I are dimerized [Fig. 1(b)]. Shown in Fig. 1 are the main structural parameters calculated for the two polymorphs. These structures are in excellent agreement with the experimental information [11,33]. For instance, the Nb-Nb repeat distance in polymorph V is found to be 3.340 Å, whereas in polymorph I the Nb-Nb distances are 3.020 and 3.749 Å, showing a strong dimerization. The experimental

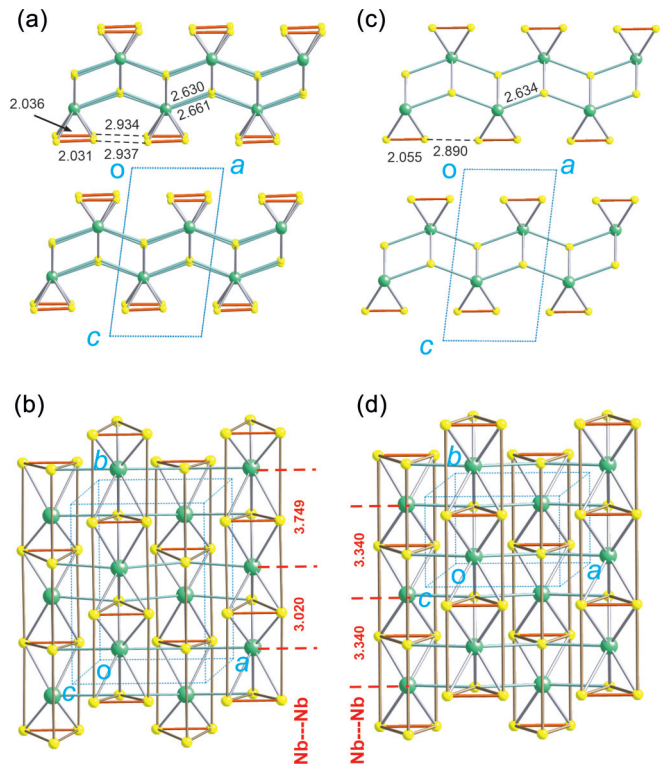


FIG. 1. DFT optimized structures for two structurally related ambient pressure NbS<sub>3</sub> polymorphs, NbS<sub>3</sub>-I [(a) and (b)] and NbS<sub>3</sub>-V [(c) and (d)]. The distances noted are those of the DFT optimized structures. In (b) and (d) the long S-S distances have been drawn to emphasize the trigonal prismatic coordination of the Nb atoms.

values are 3.358 for polymorph V and 3.045 and 3.702 Å for polymorph I.

An important structural observation is that in both structures one of the three S-S distances of the sulfur triangles is very short, 2.055 Å in polymorph V and 2.031/2.036 Å in polymorph I (experimental values, 2.019 for polymorph V and 2.050/2.050 Å for polymorph I). Such a distance is compatible with an S-S single bond so that in terms of electron counting, the S-S bonded pair should be considered as S<sub>2</sub><sup>2-</sup> and the isolated S atom as S<sup>2-</sup>. The Nb atoms are thus formally Nb<sup>4+</sup>, i.e., Nb *d*<sup>1</sup>. The observation of a semiconducting behavior for polymorph I, together with a doubling of the periodicity along the chain direction where Nb-Nb short and long distances alternate, may be considered as the outcome of a Peierls transition due to the occurrence of a formally half-filled band that opens a band gap at the Fermi level upon dimerization.

Polymorph V is found to be 211.2 meV/NbS<sub>3</sub> less stable than polymorph I, which is the most stable of all studied NbS<sub>3</sub> polymorphs [10]. The calculated band structures for the two polymorphs are shown in Fig. 2. The dimerized polymorph I exhibits a band gap of 0.99 eV that is in excellent agreement with experimental data (0.83–1.1 eV) [5,34], whereas a metallic character is predicted for polymorph V. These results bring to the fore an obvious question: Why should both polymorphs be stable (they have both been observed at ambient temperature and pressure conditions)? Since they are related through a simple Peierls dimerization and polymorph V is calculated to

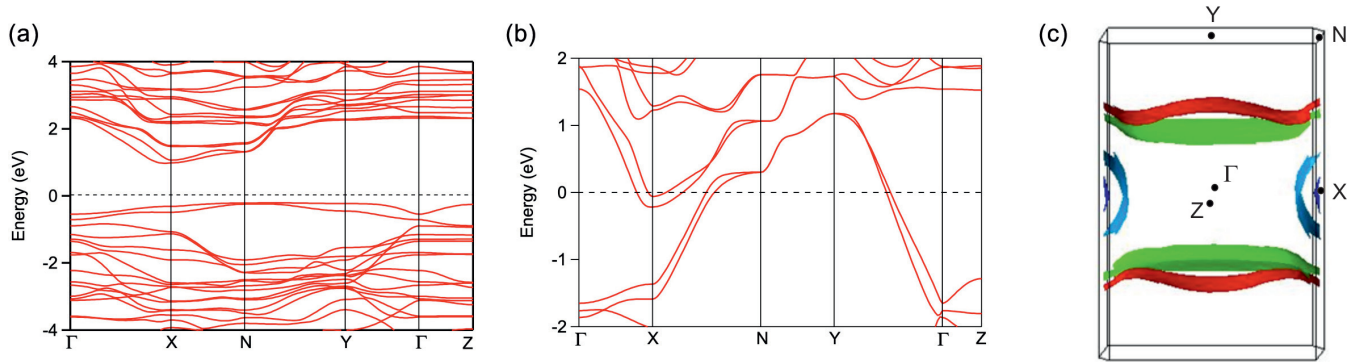


FIG. 2. Band structures for the NbS<sub>3</sub> polymorphs I (dimerized) (a) and V (nondimerized) (b) at ambient pressure where  $\Gamma = (0, 0, 0)$ ,  $X = (1/2, 0, 0)$ ,  $Y = (0, 1/2, 0)$ ,  $N = (1/2, 1/2, 0)$ , and  $Z = (0, 0, 1/2)$  in units of the reciprocal-lattice vectors. Note the larger energy scale in (a). (c) Fermi surface of polymorph V at ambient pressure.

be less stable than the dimerized one, only polymorph I should be observed in these conditions.

To have some hint regarding this question, we must turn to the band structure and Fermi surface (FS) of the nondimerized polymorph. The key feature is that for the band structure of polymorph V [Fig. 2(b)] there is an avoided crossing along the X to N line just at the Fermi level. The avoided crossing implicates strongly dispersive and flat bands (note that the bands occur in pairs because there are two equivalent NbS<sub>3</sub> units per unit cell). The strongly dispersive pair of bands rising from X to N is mostly built from the Nb  $d_{z^2}$  orbitals. If it were not for the avoided crossing, this pair of bands would be half-filled and the simple Peierls-type dimerization argument would apply. However, the avoided crossing at the Fermi level slightly empties the Nb  $d_{z^2}$  bands, which are no longer half-filled. The flat pair of bands along X-N, which has been slightly populated, is strongly dispersive along the interchain  $a^*$  direction ( $\Gamma$ -X line) because it is based on the Nb  $d_{xy}$  orbitals (we use a local coordinate system centered on the Nb atoms with the  $x$  and  $z$  directions along the  $a$  and  $b$  crystallographic axes), which point towards the capping S atoms of the adjacent NbS<sub>3</sub> chains (see Fig. 3). Consequently, they strongly interact with the S  $p_x$  orbitals, thus leading to the strong dispersion along  $\Gamma$ -X. Because of this hybridization,

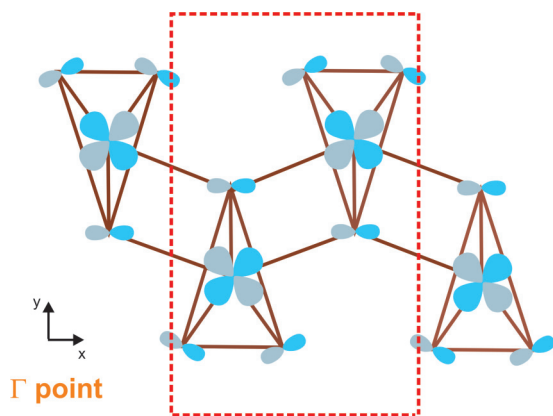


FIG. 3. Nature of the band introducing interchain coupling into the Fermi surface of the NbS<sub>3</sub> polymorph V (the crystal orbital shown is that for the  $\Gamma$  point).

interchain interactions are introduced in the states around the Fermi level. As clearly seen in the calculated FS of polymorph V [Fig. 2(c)], although in large parts of the Fermi surface the *formally* half-filled strongly nested Nb  $d_{z^2}$  pair of bands are dominant (red and green components of the FS), the planes near the border of the BZ along the  $a^*$  direction contain closed pockets (blue components of the FS) as a result of the substantial interchain interactions.

We thus conclude that the classical Peierls-type description of the mechanism of the dimerized structure of polymorph I is not really correct. If some modulation destroying the flat portions of the FS stabilizes the system, it must be incommensurate because of the electron transfer to the Nb  $d_{xy}$  type band and not a simple dimerization as observed experimentally. In addition, because of the pockets around the X point, the system will still be metallic after the transition. Recently, it has been reported that some crystals of NbS<sub>3</sub> exhibit a structure with an incommensurate periodicity along the chain direction not far from doubling [35]. Although several possibilities can be invoked to explain this observation, for the time being it is tempting to propose that the above FS nesting mechanism may be at the origin of this observation.

Because of the avoided crossing, as we approach the border of the BZ along the  $a^*$  direction (i.e., the intralayer interchain direction) the standard Peierls-type picture is strongly perturbed because of the interchain interactions occurring for wave vectors in that part of the BZ. Thus, in order for the commensurate dimerization to occur, there must be some additional distortion that removes this interchain coupling from the FS (essentially a breathing of the S-Nb-S capping angle which will destabilize the Nb  $d_{xy}$ -based antibonding band). Only then does the classical picture of well-nested half-filled Nb  $d_{z^2}$  bands hold, and the dimerization may occur. It is because of the unexpected injection of substantial interchain interaction within the Nb  $d_{z^2}$  bands that polymorph V is stable. However, polymorph I is more stable because of the additional stabilizing metal-metal interactions.

At this point, it is useful to recall the metal-to-insulator transition occurring in both NbO<sub>2</sub> and VO<sub>2</sub>, which are also  $d^1$  systems and where the tendency towards a dimerization is partially hidden by interchain interactions occurring in the metallic rutile-type structure. Detailed DFT calculations for NbO<sub>2</sub> [36] have shown that an electron redistribution

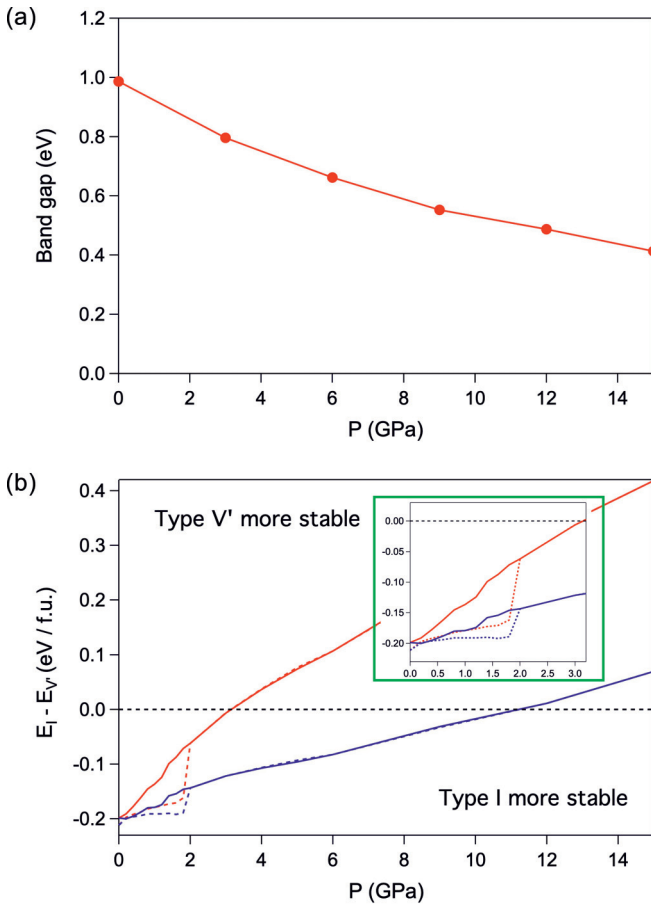


FIG. 4. (a) Evolution of the band gap of the semiconducting  $\text{NbS}_3$  dimerized polymorph under pressure. (b) Evolution of the relative stability of the dimerized and nondimerized structurally related polymorphs as a function of pressure. The blue and red curves refer to internal energy and enthalpy differences, respectively. Solid lines correspond to the V' polymorph while dashed ones correspond to the V polymorph.

emptying  $d$  orbitals different from those making  $\sigma$  metal-metal interactions occurs concomitantly with the structural dimerization. In  $\text{VO}_2$  the same type of charge redistribution (i.e., dimensionality change) occurs [37,38], but the situation is more complex because of the importance of

electron-electron interactions, spin-charge decoupling, and the competition between several transitions [39].

#### IV. EVOLUTION OF THE RELATIVE STABILITY OF THE TWO POLYMORPHS UNDER PRESSURE

For reasons that will become clear later, from the time being we will refer to polymorphs I and V for dimerized and nondimerized, respectively. Shown in Fig. 4(a) is the evolution of the calculated band gap of the semiconducting dimerized polymorph as a function of pressure. As mentioned, the calculated value at ambient pressure (0.99 eV) is in excellent agreement with the experimental value (0.83–1.1 eV) [5,34]. The evolution of the band structure with pressure is simply a rigid shift decreasing the gap [compare Figs. 2(a) and 5(a)]. The gap decreases smoothly with pressure but even at 15 GPa is only reduced to a value slightly smaller than one-half (0.41 eV) the value at ambient pressure. Thus, a progressive closing of this band gap does not provide a convincing explanation for the metallization under pressure. The band-gap underestimation of the PBE functional used in previous studies [21] is probably at the origin of this unlikely conclusion.

As shown in Fig. 4(b), the evolution of the relative stability of the two polymorphs under pressure (blue curve) exhibits a crossing between 10 and 12 GPa so that the nondimerized polymorph becomes the stable one. In addition, the band structure of this polymorph after the crossing is consistent with a metallic behavior [Fig. 5(b)]. When the enthalpy difference (red curve) is considered to correctly evaluate the pressure at which the phase transition should take place, the crossing occurs sooner, between 3 and 4 GPa. Thus we believe that the inversion of the relative stability of the two polymorphs is likely to be at the origin of the pressure-induced metallization of  $\text{NbS}_3$ .

We report in Tables I and II the evolution of the important structural parameters (i.e., those outlined in Fig. 1) with pressure. Although the relative variation of the volume from ambient pressure to 15 GPa is similar, there is an important difference between the behavior of the two polymorphs. All structural parameters change smoothly in the case of the dimerized polymorph (Table II), but there is a strong change of the bonded S-S distance and the associated interchain S...S contact between 1 and 2 GPa in the case of the nondimerized

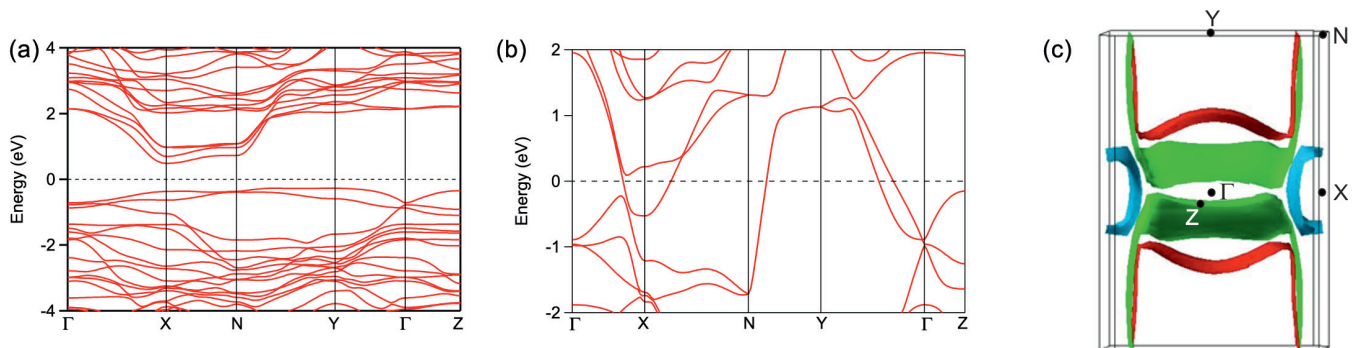


FIG. 5. Band structures for the dimerized (a) and nondimerized (b) polymorphs at 12 GPa where  $\Gamma = (0, 0, 0)$ ,  $X = (1/2, 0, 0)$ ,  $Y = (0, 1/2, 0)$ ,  $N = (1/2, 1/2, 0)$ , and  $Z = (0, 0, 1/2)$  in units of the reciprocal-lattice vectors. (c) Calculated Fermi surface at 12 GPa.

TABLE I. Evolution with pressure (0–15 GPa) of the important structural parameters of the nondimerized polymorph.

Pressure (GPa)	0	1	2	3	6	9	12	15
S-S (Å)	2.055	2.061	2.291	2.295	2.301	2.307	2.309	2.310
S...S (Å)	2.890	2.856	2.513	2.497	2.461	2.432	2.410	2.388
Nb-S <sub>cap</sub> (Å)	2.634	2.621	2.606	2.600	2.585	2.571	2.558	2.544
S <sub>cap</sub> -Nb-S <sub>cap</sub> (deg)	139.6	139.4	134.2	134.2	134.2	134.3	134.6	134.8
Nb-Nb (Å)	3.340	3.323	3.323	3.316	3.291	3.271	3.249	3.230
V (Å <sup>3</sup> )	151.77	147.90	140.60	138.63	134.16	130.33	127.04	124.24

polymorph. There is also a noticeable change in the S-Nb-S capping angle. After 2 GPa, the variations are smooth until 15 GPa. This structural change, mostly affecting the ...S-S...S-S... chains formed by the outer sulfur atoms of the triangles, has an important influence on the nature of the metallic state of the nondimerized polymorph (Fig. 6). Whereas the band structure at 1 GPa is almost the same as that at ambient pressure [compare Figs. 2(a) and 6(a)], that at 2 GPa exhibits important differences [compare Figs. 2(b) and 6(b), respectively]. The pair of flat bands occurring at the Fermi level at 1 GPa have been shifted down and appear around  $-1.2$  eV at 2 GPa.

The band structure of Fig. 6(b) is strongly reminiscent of another NbS<sub>3</sub> polymorph theoretically predicted in Ref. [10] (polymorph V'), which also contains uniform Nb chains. Looking at the structural details in Table I for pressures higher than 2 GPa, it is clear that the short S-S distance and the associated interchain S...S contact which are very different at ambient pressure [ $\sim 2.055$  and  $\sim 2.890$  Å; see Fig. 1(b)] become considerably more similar at pressures larger than 2 GPa (for instance, 2.295 and 2.497 Å at 3 GPa and 2.310 and 2.388 Å at 15 GPa). This coincides with the structural characteristics of the previously predicted NbS<sub>3</sub> polymorph V', which is also nondimerized. Thus, a third polymorph (see Fig. 7) comes into play, and we must consider in more detail the region between ambient pressure and 3 GPa. Thus from now on we will differentiate between the two nondimerized polymorphs V and V'.

A careful study of this low-pressure region [see the inset in Fig. 4(b)] of the phase diagram showed that polymorph V is only stable for pressures below 1.9 GPa. After this pressure, the structure of polymorph V collapses into that of polymorph V'. In fact, this polymorph is slightly more stable than polymorph V even at ambient pressure (12.5 meV/f.u.). From ambient pressure to 1.8 GPa the internal energy difference between polymorphs V and V' practically does not change, but polymorph V becomes less favored when enthalpy is considered because of the smaller volume of polymorph V'.

Increasing the pressure above 1.9 GPa, polymorph V is not found anymore and polymorph I is destabilized with respect to polymorph V' such that the latter becomes the preferred polymorph around 11 GPa on internal energy grounds, but around 3 GPa when enthalpy is considered.

To summarize, according to our study the observed polymorph V is only stable for a narrow region around ambient pressure, the semiconducting polymorph I is the more stable polymorph up to 3 GPa, but then the as yet noncharacterized polymorph V' becomes more stable up to pressures around 15 GPa. Because of the quite small energy difference between the two nondimerized polymorphs, we cannot firmly conclude which of the two, V or V', is the lower-energy one at ambient pressure, and thus if the metallization process we are describing implicates just two (I and V') or three (I, V, and V') different polymorphs, although for the present purpose it is not relevant.

Summarizing the previous discussion, based on the fair agreement between the calculated and experimental transition pressures, the strong structural relationship of the two polymorphs, and the metallic character of polymorph V', we believe that the proposed mechanism for the insulator-to-metal pressure-induced transition of NbS<sub>3</sub> is a reasonable one in contrast with the so far proposed progressive closing of the band gap of polymorph I.

The calculated FSs for the new polymorph V' at 2 and 12 GPa are shown in Figs. 6(c) and 5(c), respectively. These Fermi surfaces are very similar, as could be expected from the smooth variation of the band structure under pressure [compare the 12 and 2 GPa band structures in Figs. 5(b) and 6(b), respectively]. Essentially the polymorph V' FS results from the hybridization of a pair of warped 1D FSs perpendicular to the  $b^*$  direction (see the two strongly rising bands along  $\Gamma$ -Y based on the Nb  $d_{z^2}$  orbitals) and another pair of warped 1D FSs perpendicular to the  $a^*$  direction (see the two strongly rising bands along N-Y based on the Nb  $d_{xy}$  orbitals with a substantial contribution of the S  $p$  orbitals very similar to that

TABLE II. Evolution with pressure (0–15 GPa) of the important structural parameters of the dimerized polymorph.

Pressure (GPa)	0	3	6	9	12	15
S-S (Å)	2.031/2.036	2.030/2.036	2.029/2.036	2.306/2.036	2.307/2.037	2.038/2.038
S...S (Å)	2.937/2.934	2.860/2.859	2.806/2.799	2.756/2.748	2.716/2.704	2.681/2.664
Nb-S <sub>cap</sub> (Å)	2.661/2.629	2.622/2.592	2.593/2.563	2.567/2.510	2.545/2.519	2.526/2.500
S <sub>cap</sub> -Nb-S <sub>cap</sub> (deg)	137.9/141.6	137.5/141.0	137.2/140.5	136.8/140.0	136.6/139.7	136.2/139.2
Nb-Nb (Å)	3.028/3.719	3.013/3.694	2.999/3.672	2.987/3.653	2.975/3.634	2.968/3.617
V (Å <sup>3</sup> )	306.28	289.59	278.43	269.76	262.39	255.93

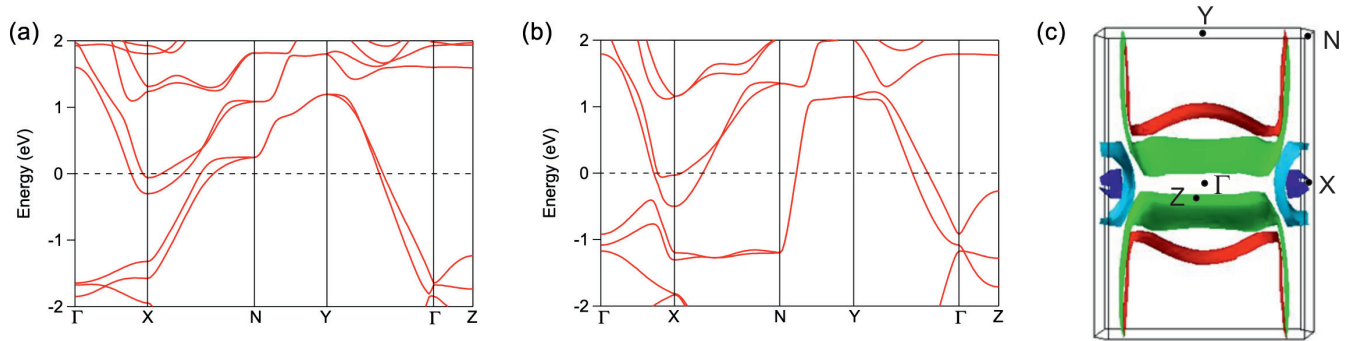


FIG. 6. Band structure for the nondimerized polymorph at 1 GPa (a) and 2 GPa (b), where  $\Gamma = (0, 0, 0)$ ,  $X = (1/2, 0, 0)$ ,  $Y = (0, 1/2, 0)$ ,  $N = (1/2, 1/2, 0)$ , and  $Z = (0, 0, 1/2)$  in units of the reciprocal-lattice vectors. (c) Calculated Fermi surface at 2 GPa.

shown in Fig. 3). The shape of these FSs may appear a bit complex at first glance because of the occurrence of avoided band crossings not far from the  $X$  point. As explained above for polymorph V (Sec. III), it is around that zone of the BZ that the strong hybridization between the intrachain and interchain bands occurs. Since the intra- and interchain bands are 1D along perpendicular directions, these bands introduce closed FS components around  $X$ . However, the position of the two bands subtly varies with pressure, thus influencing the shape of the FS in that zone. At high pressure [Fig. 5(b)] one of the two bands lies slightly above the Fermi level, but around the pressure of the transition [Fig. 6(b)] this band slightly crosses the Fermi level. Thus there is only one closed component around  $X$  in the first case but two in the second. However, when the contributions of all bands are represented together as in Figs. 6(c) and 5(c), the description of the FS as resulting from the interaction of two pairs of warped 1D FS components becomes clear.

Thus, the metallic state stabilized after the transition is predicted to be essentially a 2D metal with good conductivity in the  $ab$  plane but a considerably smaller one along the interlayer direction. However, because of the occurrence of substantial rather flat portions, it could exhibit resistivity anomalies as a result of a nesting process along both the  $a^*$  and/or  $b^*$  directions so that the existence of further incommensurate metallic phases cannot be discarded. We remind

the reader of the recent observation of  $\text{NbS}_3$  phases with an incommensurate, although not far from double cell parameter along the chains [35]. Although without a more in-depth study it would be premature to ascribe this observation to the FS instability of polymorph V discussed in Sec. III, it certainly lends plausibility to the suggestion of the possible occurrence of new  $\text{NbS}_3$  metallic phases with incommensurate periodicity. Note that the presence of closed portions in the FS around the  $X$  point could lead to pressure-dependent magnetoresistance oscillations. A rich physics of  $\text{NbS}_3$  under pressure is probably still uncovered.

The difference between the metallic states of polymorphs V and V' as well as the origin of the insulator-to-metal transition can now be easily understood. In polymorph-V the bottom of the bands associated with the interchain interactions [i.e., the strongly dispersive bands along  $\Gamma$ - $X$  in Figs. 2(b) and 6(a)] occurs slightly below  $X$  so that they only introduce a relatively small 2D component in the FS [see Fig. 2(c)]. However, in polymorph V' the bands bringing the interchain interactions have a considerably larger slope, and their bottom occurs (after an avoided crossing) around 1 eV lower. This introduces a considerably larger contribution of the interchain interactions so that their 1D nature clearly appears. As mentioned before, these bands bear important S  $p$  contributions from the outer S atoms pointing towards each other (see Fig. 3). When the phase changes from  $\Gamma$  to  $X$ , the S-S interchain interactions become bonding whereas the intrachain ones keep their antibonding character. Since pressure shortens the interchain contacts, the band is stabilized, it becomes more populated, and it precipitates the equalization of the S-S contacts because of the bonding/antibonding character of the inter/intra S-S interactions. This is the origin of the sulfur chains and the main reason for the stabilization of the polymorph. In chemical terms, pressure favors the chemical reduction of the S-S bonds in polymorph V, disfavoring this polymorph and stabilizing the V' one. In contrast, polymorph I has this band far from the Fermi level because of the formation of the metal-metal bonds. Compression induces strong  $S_p$ - $S_p$  interchain repulsions in the valence band, thus disfavoring this polymorph. Again, the pressure dependence of the  $\text{NbS}_3$  structure nicely illustrates the subtle trading between the S-S bond reduction and the metal-metal bonding abilities of this layered system [10].

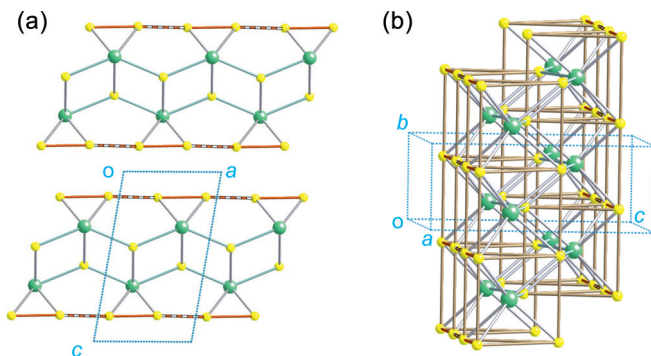


FIG. 7. Top (a) and side (b) views of the  $\text{NbS}_3$ -V' polymorph. Note the occurrence of sulfur chains in the outer part of the layers along the  $a$ -direction. In (b) the long S-S distances have been drawn to emphasize the trigonal prismatic coordination of the Nb atoms.

## V. CONCLUDING REMARKS

The present first-principles study suggests that the reported insulator-to-metal transition in NbS<sub>3</sub> is not due to a progressive closing of the initial band gap, as previously proposed, but to the inversion of the relative stability of different, dimerized, and nondimerized, polymorphic structures (NbS<sub>3</sub> polymorphs I, V, and V') under pressure. According to this study, the recently observed polymorph V would only be stable for a narrow region around ambient pressure and is not the more stable polymorph with regular Nb-Nb chains. The semiconducting polymorph I is the more stable polymorph up to ≈3 GPa, but then the as yet noncharacterized polymorph V' becomes more stable up to pressures around 15 GPa. The FS of polymorph V' exhibits nested portions that are suggestive of the possible occurrence of further incommensurate NbS<sub>3</sub> phases. The insulator-to-metal transition is ascribed to the competition between the S-S bond reduction and metal-metal bonding capabilities of NbS<sub>3</sub> under pressure.

## ACKNOWLEDGMENTS

This work was supported by Spanish MICIU (Grants No. PID2022-139776NB-C61 and No. PID2021-128217NB-I00) and Generalitat de Catalunya (Grants No. 2021SGR01519 and No. 2021SGR00286). E.C. acknowledges the support of the Spanish MICIU through the Severo Ochoa FUNFUTURE (CEX2019-000917-S) Excellence Centre distinction. P.A. acknowledges the support from the Maria de Maeztu Units of Excellence Program (CEX2021-001202-M) and the MEC-ANID program (Grant No. 80190101) for a stay at the Universidad Católica del Norte. S.C. was supported by FONDECYT, Chile (project 1221697) and was partially supported by the supercomputing infrastructure of the NLHPC (ECM-02). S.C. would also like to thank “Núcleo de modelación y simulación científica (NMSC)” No. 7 UCN-VRIDT 076/2020, and “Núcleo de materiales funcionales” No. 8 UCN-VRIDT 076/2020 for scientific support. We thank Professor V. Pokrovskii for communication of unpublished results.

- [1] *Crystal Chemistry and Properties of Materials with Quasi-One-Dimensional Structures*, edited by J. Rouxel (Reidel, Dordrecht, The Netherlands, 1986).
- [2] P. Monceau, *Adv. Phys.* **61**, 325 (2012).
- [3] J. Rouxel and C. Schlenker, in *Charge Density Waves in Solids*, Modern Problems in Condensed Matter Sciences, edited by L. P. Gorkov and C. Grüner (North Holland, Amsterdam, 1989), pp. 15–83.
- [4] P. Monceau, N. P. Ong, A. M. Portis, A. Meerschaut, and J. Rouxel, *Phys. Rev. Lett.* **37**, 602 (1976).
- [5] J. O. Island, A. J. Molina-Mendoza, M. Barawi, R. Biele, E. Flores, J. M. Clamagirand, J. R. Ares, C. Sánchez, H. S. J. van der Zant, R. D'Agosta, I. J. Ferrer, and A. Castellanos-Gomez, *2D Mater.* **4**, 022003 (2017).
- [6] S. Takahashi, T. Sambongi, J. W. Brill, and W. Roark, *Solid State Commun.* **49**, 1031 (1984).
- [7] R. Yomo, K. Yamaya, M. Abliz, M. Hedo, and Y. Uwatoko, *Phys. Rev. B* **71**, 132508 (2005).
- [8] A. Patra and C. S. Rout, *RSC Adv.* **10**, 36413 (2020).
- [9] J. Dai, M. Li, and X. C. Zeng, *WIREs Comput. Mol. Sci.* **6**, 211 (2016).
- [10] S. Conejeros, B. Guster, P. Alemany, J.-P. Pouget, and E. Canadell, *Chem. Mater.* **33**, 5449 (2021).
- [11] J. Rijnsdorp and F. Jellinek, *J. Solid State Chem.* **25**, 325 (1978).
- [12] S. Furuse, L. Brattås, and A. Kjekshus, *Acta Chem. Scand.* **29a**, 623 (1975).
- [13] Z. Z. Wang, P. Monceau, H. Salva, C. Roucau, L. Guemas, and A. Meerschaut, *Phys. Rev. B* **40**, 11589 (1989).
- [14] E. Zupanič, H. J. P. van Midden, M. A. van Midden, S. Šturm, E. Tchernychova, V. Y. Pokrovskii, S. G. Zybtev, V. F. Nasretdinova, S. V. Zaitsev-Zotov, W. T. Chen, W. W. Pai, J. C. Bennett, and A. Prodan, *Phys. Rev. B* **98**, 174113 (2018).
- [15] J. L. Hodeau, M. Marezio, C. Roucau, R. Ayroles, A. Meerschaut, J. Rouxel, and P. Monceau, *J. Phys. C* **11**, 4117 (1978).
- [16] S. G. Zybtev, V. Y. Pokrovskii, V. F. Nasretdinova, S. V. Zaitsev-Zotov, V. V. Pavlovskiy, A. B. Odobesco, W. W. Pai, M.-W. Chu, Y. G. Lin, E. Zupanič, H. J. P. van Midden, S. Šturm, E. Tchernychova, A. Prodan, J. C. Bennett, I. R. Mukhamedshin, O. V. Chernysheva, A. P. Menushenkov, V. B. Loginov, B. A. Loginov *et al.*, *Phys. Rev. B* **95**, 035110 (2017).
- [17] M. A. Bloodgood, P. Ghafouri, Y. Wei, and T. T. Salguero, *Appl. Phys. Lett.* **120**, 173103 (2022).
- [18] C. An, P. Lu, X. Chen, Y. Zhou, J. Wu, Y. Zhou, C. Park, C. Gu, B. Zhang, Y. Yuan, J. Sun, and Z. Yang, *Phys. Rev. B* **96**, 134110 (2017).
- [19] X. Zhong, M. Zhang, L. Yang, X. Qu, L. Yang, J. Yang, and H. Liu, *Comput. Mater. Sci.* **158**, 192 (2019).
- [20] B. Yue, W. Zhong, W. Deng, T. Wen, Y. Wang, Y. Yin, P. Shan, J.-T. Wang, X. Yu, and F. Honh, *J. Am. Chem. Soc.* **145**, 1301 (2023).
- [21] M. Abdel-Hafiez, R. Thiyagarajan, A. Majumdar, R. Ahuja, W. Luo, A. N. Vasiliev, A. A. Maarouf, S. G. Zybtev, V. Y. Pokrovskii, S. V. Zaitsev-Zotov, V. V. Pavlovskiy, W. W. Pai, W. Yang, and L. V. Kulik, *Phys. Rev. B* **99**, 235126 (2019).
- [22] E. M. Dizhur, M. A. Il'ina, and S. V. Zaitsev-Zotov, *JETP Lett.* **86**, 132 (2007).
- [23] P. Hohenberg and W. Kohn, *Phys. Rev.* **136**, B864 (1964).
- [24] W. Kohn and L. J. Sham, *Phys. Rev.* **140**, A1133 (1965).
- [25] R. Dovesi, A. Erba, R. Orlando, C. M. Zicovich-Wilson, B. Civalleri, L. Maschio, M. Rerat, S. Casassa, J. Baima, S. Salustro, and B. Kirtman, *WIREs Comput. Mol. Sci.* **8**, e1360 (2018).
- [26] See <http://www.crystal.unito.it> for details on the CRYSTAL code, Gaussian Basis Sets, Computational schemes, etc., (2019), accessed December 2023.
- [27] R. Dovesi, V. R. Saunders, C. Roetti, R. Orlando, C. M. Zicovich-Wilson, F. Pascale, B. Civalleri, K. Doll, N. M. Harrison, I. J. Bush, P. D'Arco, M. Llunell, M. Causà, Y. Noël, L. Maschio, A. Erba, M. Rerat, S. Casassa, CRYSTAL17 (2017) CRYSTAL17 User's Manual. University of Torino, Torino.
- [28] A. V. Krukau, O. A. Vydrov, A. F. Izmaylov, and G. E. Scuseria, *J. Chem. Phys.* **125**, 224106 (2006).

- [29] S. Dall'Olio, R. Dovesi, and R. Resta, *Phys. Rev. B* **56**, 10105 (1997).
- [30] M. F. Peintinger, D. Vilela Oliveira, and T. Bredow, *J. Comput. Chem.* **34**, 451 (2013).
- [31] R. Dovesi, R. Orlando, C. Roetti, V. R. Saunders, and C. M. Zicovich-Wilson, *Z. Kristallogr. Cryst. Mater.* **220**, 571 (2005).
- [32] H. J. Monkhorst and J. D. Pack, *Phys. Rev. B* **13**, 5188 (1976).
- [33] M. A. Bloodgood, P. Wei, E. Aylan, K. N. Bozhilov, A. A. Balandin, and T. T. Salguero, *APL Mater.* **6**, 026602 (2018).
- [34] M. E. Itkis, F. Y. Nad, and F. Levy, *Synth. Met.* **43**, 3969 (1991).
- [35] S. G. Zybtev, N. Y. Tabachkova, V. Y. Pokrovskii, S. A. Nikonov, A. A. Maizlakh, and S. V. Zaitsev-Zotov, *JETP Lett.* **114**, 40 (2021).
- [36] V. Eyert, *Europhys. Lett.* **58**, 851 (2002).
- [37] V. Eyert, *Phys. Rev. Lett.* **107**, 016401 (2011).
- [38] V. Eyert, *Ann. Phys.* **514**, 650 (2002).
- [39] J.-P. Pouget, *C. R. Phys.* **22**, 37 (2021).